Magnetic-field-induced optical anisotropy in ferrofluids: A time-dependent light-scattering investigation

Corneliu Rablau and Prem Vaishnava
Department of Physics, Kettering University, Flint, Michigan 48504, USA

Chandran Sudakar, Ronald Tackett, Gavin Lawes, and Ratna Naik
Department of Physics and Astronomy, Wayne State University, Detroit, Michigan 48201, USA
(Received 11 July 2008; published 6 November 2008)

We report an experimental investigation of time dependent anisotropic light scattering by an aqueous suspension of tetramethyl ammonium hydroxide coated Fe_3O_4 nanoparticles ($\sim$6 nm) under the ON-OFF transient of an external dc magnetic field. The study employs the synchronized recording and measurement of the two magnetic-field-induced light-scattering patterns produced by two identical orthogonal He-Ne laser beams passing through the ferrofluid sample and propagating parallel and perpendicular to the applied field, respectively. From these patterns, we extract the time dependence of the induced optical anisotropy, which provides a measure of the characteristic time scale and kinematic response for field-induced structure formation in the sample. We propose that the time evolution of the scattering patterns, which is very fast at short times and significantly slower at long times, can be explained using a model based on a two-stage chain formation and coarsening processes.

DOI: 10.1103/PhysRevE.78.051502 PACS number(s): 83.80.Gv, 82.70.$-$y, 61.20.$-$p, 89.75.Fb

I. INTRODUCTION

It is largely accepted that when a dc electric or magnetic field is applied to a colloidal suspension consisting of particles with a dielectric constant or magnetic permeability different from that of the carrier liquid, the particles polarize and interact causing them to align along the field lines and to form chainlike and columnlike structures [1–11]. The formation of these field-induced chainlike structures and their effect on relevant physical properties of the suspension has been studied theoretically through extensive numerous computer simulations [9–20] and experimentally through birefringence and scattering dichroism measurements [5,6,21], longitudinal magneto-optic effects such as circular birefringence (Faraday rotation) and circular dichroism (Faraday ellipticity) [22,23], Raman scattering [1], visible light and/or x-ray scattering [4,6,24,25], and optical attenuation or transmission measurements [3,9,26,27]. On a fundamental level, these investigations are important because there is a growing interest in the study of light propagation and scattering through these complex media stemming from the realization that many electronic effects in condensed matter physics have their analog in the propagation of electromagnetic waves in strong scattering media. Among these are the photonic Hall effect [28], photonic magnetoresistance [29], localization of light [30], and zero forward scattering and enhancement of coherent backscattering of light [31].

Theoretical views on chain formation and coarsening in field-responsive colloidal suspensions generally involve the temporal separation of two processes: chain formation and column formation. In this framework, particles having a dipole (or multipole) moment first aggregate along field lines to form chains. At longer times, the chains then aggregate to form columns, which further aggregate into even thicker columns. This theoretical view was first developed by Halsey and Toor (HT) [7], who showed that thermal fluctuations can lead to a long-range chain-chain interaction, resulting in thermally driven coarsening. The HT theory was then expanded by Martin *et al.* [9,10] to include the time scales of interaction and the effects of topological defects in chains, which can drive coarsening in the absence of thermal fluctuations (defect-driven coarsening). Using computer modeling, Martin *et al.* predicted power-law coarsening kinetics $L\sim t^{\beta}$, where $\beta\approx0.5$ for both thermally driven coarsening and defect-driven coarsening. Here, L is the characteristic column separation (transverse correlation length) and t is the time. These results were in agreement with the coarsening exponent of 0.5 ± 0.1 obtained by Martin *et al.* [10] from time-dependent light-scattering measurements on a single-scattering electrorheological fluid consisting of 0.7-μm-diameter silane-surfaced silica spheres dispersed in 4-methylcyclohexanol. Through video microscopy and direct measurement of the lateral interaction between chains using optical trapping (laser tweezers), Furst and Gast [8] further expanded HT theory and found that lateral interactions leading to chain coalescence into columns govern the long time evolution of the structures in suspension. The dominant mechanism for chain coalescence was found to depend on the concentration, the strength of the magnetic interaction, the particle polydispersity and roughness, as well as on the aggregation kinetics. This study was performed on a magnetic emulsion of single domain Fe_3O_4 nanoparticles ($\sim$10 nm) suspended in a hydrocarbon and emulsified in water, with the size of the oil drops in emulsion ranging from 0.1 to 10 μm. Hwang and Wu [24] reported a small-angle single light scattering study on a 10 to 30 μm thin film of an aqueous suspension of 0.9-μm-diam. carboxylic-acid-surfacted polystyrene spheres containing randomly oriented multigrain ferromagnetic cores. Both the longitudinal and transverse correlation of the magnetic chains was measured. The study found a series of structure changes from single particles to elongated disordered domains to transversely correlated columns as the magnetic field increases adiabatically, but their observations were somewhat different from those reported by Halsey and Toor [7], Furst and Gast [8], and Martin *et al.* [9,10].

More recently, Kruse *et al.* [4] reported a static (time-independent) two-dimensional small angle x-ray scattering (SAXS) study of the agglomeration and chain formation process in a ferrofluid consisting of a 1-mm-thick suspension of Fe_3O_4 nanoparticles having a mean diameter of about 10 nm, coated with oleic acid. The study was focused on the question of how the anisometry and size of single particles and clusters contribute to the induced structural anisotropy, and concluded that the orientation of individual nonspherical particles is relatively insignificant. Rather, the field-induced structural anisotropy—reflected in the anisotropic two-dimensional x-ray scattering—was found to be mainly due to the formation and orientation of elongated clusters with preferred alignment parallel to the field.

In spite of the relatively large number of studies described above, research dealing with the kinematics (i.e., time dependence) of the field-induced aggregation and chain formation and coarsening processes in ferrofluid suspensions are scarce in the literature. Over the last few years, optical microscopy has been used for monitoring the time evolution of the chain and cluster formation [5,6,9,32]. However, most of the studies, including the optical microscopy technique, were performed either on electrorheological or magnetorheological fluids, where the size of the dispersed phase was in the micrometer range. Furthermore, most optical transmission or scattering measurements have been performed by using a single light beam which limits the information about the chain kinematics, especially for thick samples.

In this paper we report an experimental investigation of time-dependent anisotropic light-scattering patterns produced simultaneously by two orthogonal light beams, through a surfacted, well characterized Fe_3O_4 ferrofluid (particle size 6 nm) under the off-on transient of a dc magnetic field. From the time evolution of the scattering patterns, we extract the time dependence of the induced optical anisotropy, which we propose can be explained within a model rooted in the two-stage chain formation and coarsening process introduced by Halsey and Toor [7] and expanded by Furst and Gast [8] and Martin *et al.* [9].

II. EXPERIMENTAL

A. Sample preparation

The Fe_3O_4 ferrofluid sample was prepared by coprecipitation method by mixing 4 mL of 1M $FeCl_3$ with 1 mL of 2M $FeCl_2$ solution in a beaker and adding 50 mL of 1M aqueous ammonium hydroxide solution over a period of 5 min. Fe_3O_4 (magnetite) in the form of a black precipitate was formed, which we allowed to settle at the bottom of a beaker. After decanting the clear liquid, we washed the precipitate three times with deionized water and added 2 mL of 25% tetramethyl ammonium hydroxide to prevent agglomeration of the magnetite nanoparticles. For optical scattering measurements, the sample was diluted in deionized water to a volume fraction Φ of 1%.

B. Sample characterization

The sample was characterized by x-ray diffraction (XRD), transmission electron microscopy (TEM), and superconducting quantum interference divice (SQUID) magnetometer measurements. The complete details of the characterization can be found in Ref. [33]. In brief, the XRD results showed the sample was a single phase crystalline with the expected structure of magnetite. The results from the TEM measurements for the size of the nanoparticles were fitted with a Gaussian distribution and the average diameter of the Fe_3O_4 nanoparticles in the ferrofluid sample was determined to be 6 ± 2 nm. The SQUID magnetic characterization showed superparamagnetic behavior; the magnetothermal measurements exhibited dominance of the Brownian relaxation over the Neel relaxation for heat dissipation under the influence of an ac magnetic field [33].

C. Light-scattering measurements

A schematic of the experimental setup used for the light scattering measurements is presented in Fig. 1. The ferrofluid sample in a standard quartz suprasil spectrophotometer cuvette is placed at the center of a pair of water-cooled Helmholtz coils set. A range of dc magnetic field values from 0 to 400 G were employed in these experiments, and the 3D mapping of the field revealed a field uniformity of better than 0.5% over the $\sim$2 mL volume of the ferrofluid sample. The light beams from two He-Ne lasers ($\lambda = 632.8$ nm) were transmitted through the sample simultaneously, parallel and perpendicular to the applied magnetic field, respectively. The beam diameter through the sample was $\sim$1 mm. Measurements were performed both with unpolarized and linearly polarized light having various polarization orientations with respect to the applied magnetic field. The incident laser power was in the 1 to 10 mW range, and was the same for both lasers, in any given experiment. The light path through the sample was 10 mm in both directions. The light scattered by the sample was projected onto two 220 mm $\times$ 220 mm translucent screens placed a distance of 500 mm from the center of the sample. To reflect their orientation relative to the magnetic field and to the propagation wave vector $\vec{k}_i$ of the incident light, we will call these the $\vec{k}_i \perp \vec{B}$ and $\vec{k}_i \parallel \vec{B}$ screens, respectively. This geometry combined with the dimensions and structure of the Helmholtz coils allowed scattering toward the $\vec{k}_i \parallel \vec{B}$ screen in a circular cone of half-angle $\sim 12°$ and toward the $\vec{k}_i \perp \vec{B}$ screen in a pyramid of half-angles $\sim 7.5°$ and 12° for the horizontal and vertical directions, respectively (see Fig. 1). Upon turning the magnetic field on the time-evolving patterns of the transmitted scattered light were recorded from the two screens using two synchronized digital cameras. Image analysis software was then used to convert the digital pictures into surface plots of the scattered light intensity. In a separate set of experiments, the screens were removed, and the time-dependent intensities of the light scattered in the forward direction for both $\vec{k}_i \perp \vec{B}$ and $\vec{k}_i \parallel \vec{B}$ were measured using two Newport 818-IS-1 integrating sphere detectors (entrance aperture of $\sim$1 mm). The use of an integrating sphere detector minimizes any potential

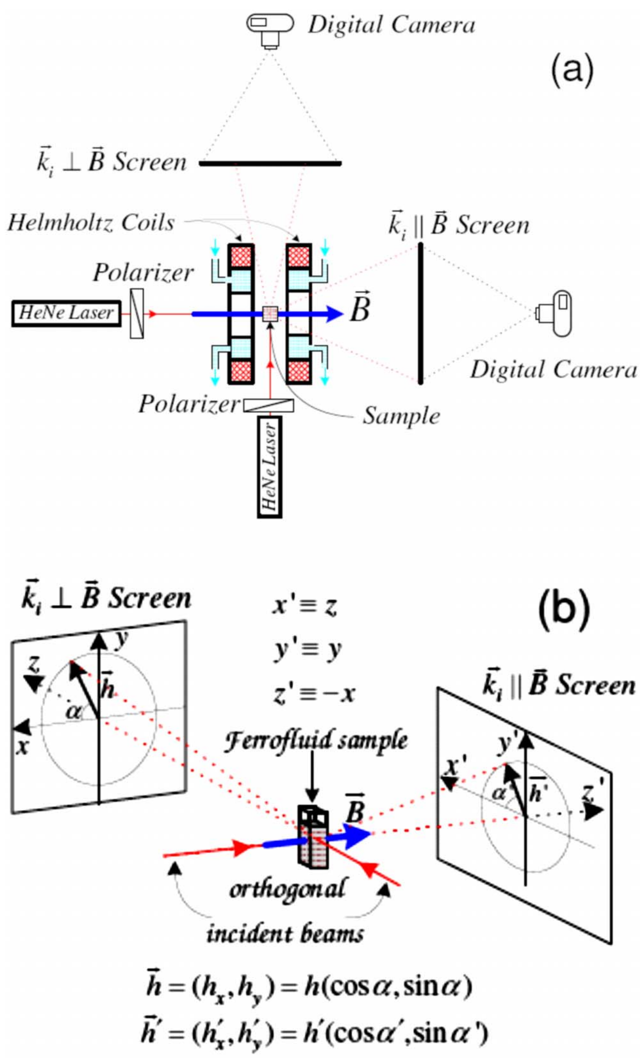

FIG. 1. (Color online) (a) Schematic of the experimental setup for synchronously recording the time-dependent light scattering patterns produced by two orthogonal light beams through a ferrofluid sample placed in a uniform magnetic field. (b) The 3D geometry of the experiment. The scattered intensity on each screen $I(\vec{h})$ or $I(\vec{h}')$ is a function of the corresponding scattering vector $\vec{h}$ or $\vec{h}'$, where $\vec{h}=(h_x,h_y)=h(\cos\alpha,\sin\alpha)$ and $\vec{h}'=(h'_x,h'_y)=h'(\cos\alpha',\sin\alpha')$.

polarization dependence of the response of the Si detector itself. All measurements were conducted at room temperature ($\sim$22 °C), with no active sample temperature control.

III. RESULTS AND DISCUSSION

We discuss the results of our experiments within a framework and system of notations similar to the ones introduced by Kruse *et al.* [4] extended to the case of the simultaneous, time-dependent measurement of two magnetic-field-induced two-dimensional light scattering patterns, produced by two identical orthogonal beams, as shown in Fig. 1(b). One must note that, in view of the long light path through the sample, the observed scattering patterns in our experiments are the result of multiple scattering rather than single scattering events. Indeed, if multiple scattering dominates the propagation, one expects the transmitted light to be completely depolarized. We confirmed the complete depolarization of the scattered light by observing the patterns through a rotating linear polarizer for the vertically and horizontally polarized incident light. The net result of the multiple scattering can be described in terms of an effective scattering wave vector $\vec{q}$, such that $\vec{k}_s=\vec{k}_i+\vec{q}$, where $\vec{k}_i$ is the wave vector of the incident light and $\vec{k}_s$ is the wave vector of the scattered light emerging from the sample cell. In the real coordinate space, the scattered intensity on each of the two screens can be described in terms of a scattering vector $\vec{h}$ or $\vec{h}'$, respectively, where $\vec{h}=(h_x,h_y)=h(\cos\alpha,\sin\alpha)$ corresponds to the $\vec{k}_i \perp \vec{B}$ screen and $\vec{h}'=(h'_x,h'_y)=h'(\cos\alpha',\sin\alpha')$ to the $\vec{k}_i \parallel \vec{B}$ screen. The effective wave scattering vector $\vec{q}$ and the coordinate-space scattering vector $\vec{h}$ are related to each other through the geometry of the experiment. For convenience and ease of notation, we will describe the scattering patterns in coordinate space, rather than the scattering wave vector space. In this representation, the scattered intensity $I(\vec{h})$ or $I(\vec{h}')$ is a function of the corresponding vector $\vec{h}$ or $\vec{h}'$.

A. Time evolution in a fixed 400 G field

Figures 2 and 3 show the scattered intensity patterns produced by two orthogonal 10 mW, y-axis-polarized red HeNe lasers on the $\vec{k}_i \perp \vec{B}$ screen (Fig. 2) and $\vec{k}_i \parallel \vec{B}$ screen (Fig. 3) in a 400 G magnetic field. With the ferrofluid sample having no prior history in a magnetic field, the field was turned on at $t=0$ and the scattered intensities were recorded at a regular time interval for 60 min. Although the wavelength used in our experiments (visible light) and the range of scattering vectors (larger scattering vectors) are different from those in the study of small angle x-ray scattering (SAXS) by Kruse *et al.* [4], we find significant similarities between the scattering patterns on the $\vec{k}_i \perp \vec{B}$ screen for the two studies. Before applying the magnetic field (i.e., at $t<0$, when $B=0$), the intensity pattern is isotropic: it does not depend on the direction of $\vec{h}=(h_x,h_y)=h(\cos\alpha,\sin\alpha)$, i.e., on the angle α. Upon turning the magnetic field on at $t=0$ (0 to 400 G transition with less than 1 s ramp-up time), an anisotropy develops: at any given magnitude h of the scattering vector, the intensity of light scattered perpendicular to the field, $I_\perp = I(h,\alpha=\pm\pi/2)$ becomes larger than the intensity of light scattered parallel to the field $I_\parallel = I(h,\alpha=0)=I(h,\alpha=\pi)$, i.e., $I_\parallel(h) < I_\perp(h)$. The pattern observed on the $\vec{k}_i \perp \vec{B}$ screen at long times—approaching a narrow, vertical line of light—has the general features of the anisotropic scattering pattern produced by a long thin cylinder [6,34]. This suggests the particles are aggregating in chainlike structures aligned with the applied field. It is also evident that the scattering anisotropy becomes stronger as time evolves. In order to provide a quantitative description of this evolution, we analyze and explain the induced anisotropy within the framework set by Kruse *et al.* [4]. According to their analysis, the scattered intensity $I(\vec{q})$ at a wave scattering vector $\vec{q}$ depends on the distribution of electron density $\rho(\vec{r})$ in the sample. Except for

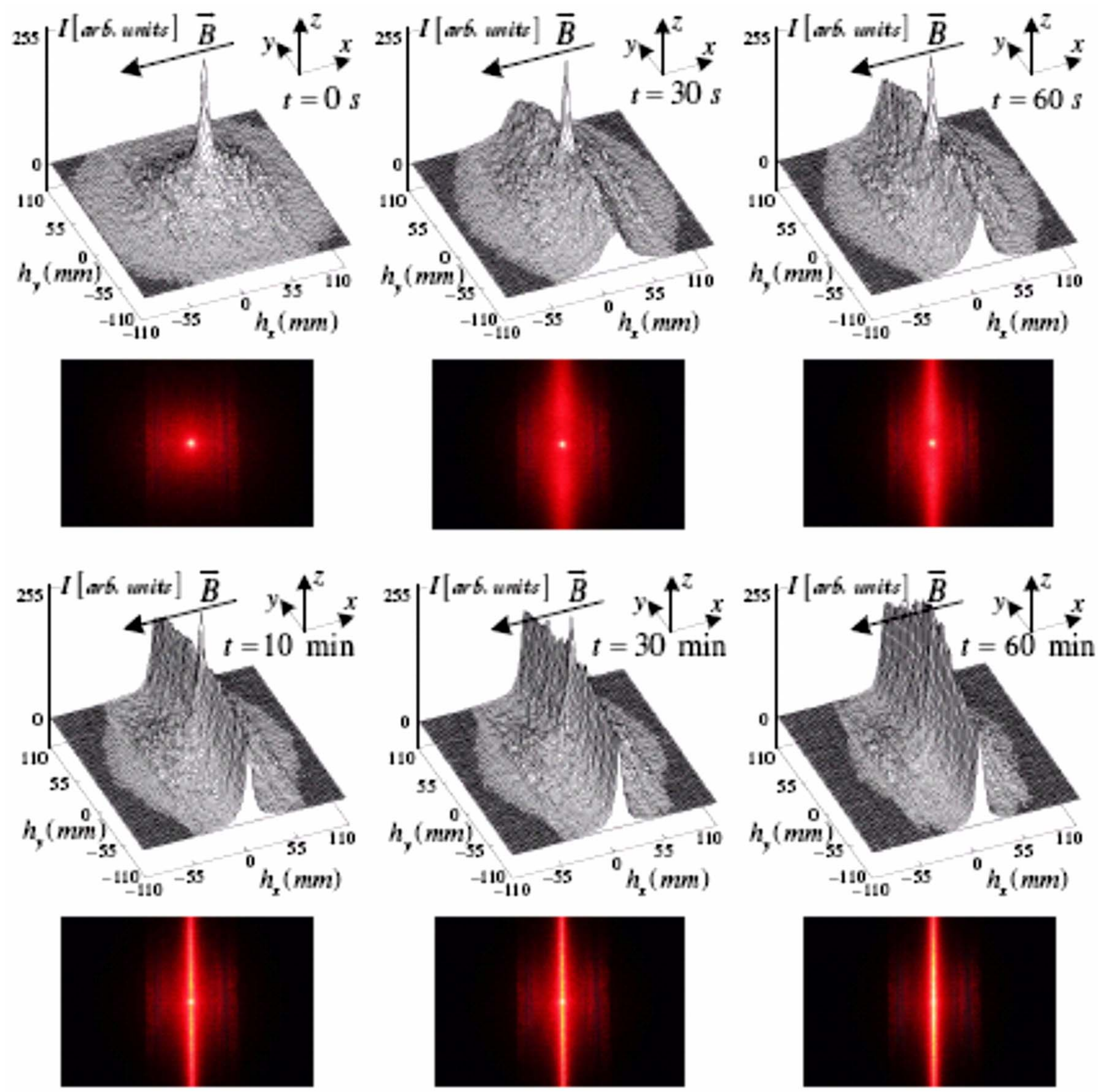

FIG. 2. (Color online) Light scattering patterns from a Fe_3O_4 ferrofluid sample and the corresponding surface plots of the scattered intensity at representative instants of time for incident light propagating perpendicular to the applied field (i.e., on the $\vec{k}_i \perp \vec{B}$ screen). The sample had no prior history in the magnetic field. The magnetic field was turned on at $t=0$, and kept at a steady dc value of 400 G throughout the entire experiment.

the case of forward scattering, the intensity distribution can be written in terms of the scattering vector $\vec{q}$ as

$$I_{h\neq 0}(\vec{q}) = I_e \int \gamma(\vec{r})\cos(q_x x)\cos(q_y y)dV, \tag{1}$$

where I_e denotes the scattering intensity of a single electron. Here, γ is the so-called "characteristic function" or "autocorrelation function" $\gamma(\vec{r})=\gamma(-\vec{r})=\Delta\rho_e(\vec{r})^*\Delta\rho_e(-\vec{r})$ and represents the convolution of the electron density contrast, i.e., of the difference between the local electron density at a point $\vec{r}$ and its volume average $\Delta\rho_e=\rho_e(\vec{r})-\bar{\rho}_e$. Since the variation of the electron density in the ferrofluid sample is mainly due to the strong contrast between the electron densities of the magnetite and the carrier liquid γ and thus the measured intensity, reflects the microstructure of the sample. On the application of a homogeneous magnetic field, the characteristic function is no longer isotropic but develops a cylindrical symmetry along the field axis. Under these conditions, the scattered intensity becomes an even periodic function of the angle α defined in Fig. 1(b), $I(h,\alpha)=I(h,\alpha\pm\pi)$. Based on this theoretical explanation, Kruse *et al.* [4] fitted their experimental data with a periodic even function of the form

$$I(h,\alpha) = I_0(h)\{1 + A(h)(\sin^2\alpha - 0.5)\}, \tag{2}$$

where $I_0(h)$ denotes the radial mean value of the scattered intensity

$$I_0(h) = \frac{I_\perp(h) + I_\parallel(h)}{2} \tag{3}$$

and

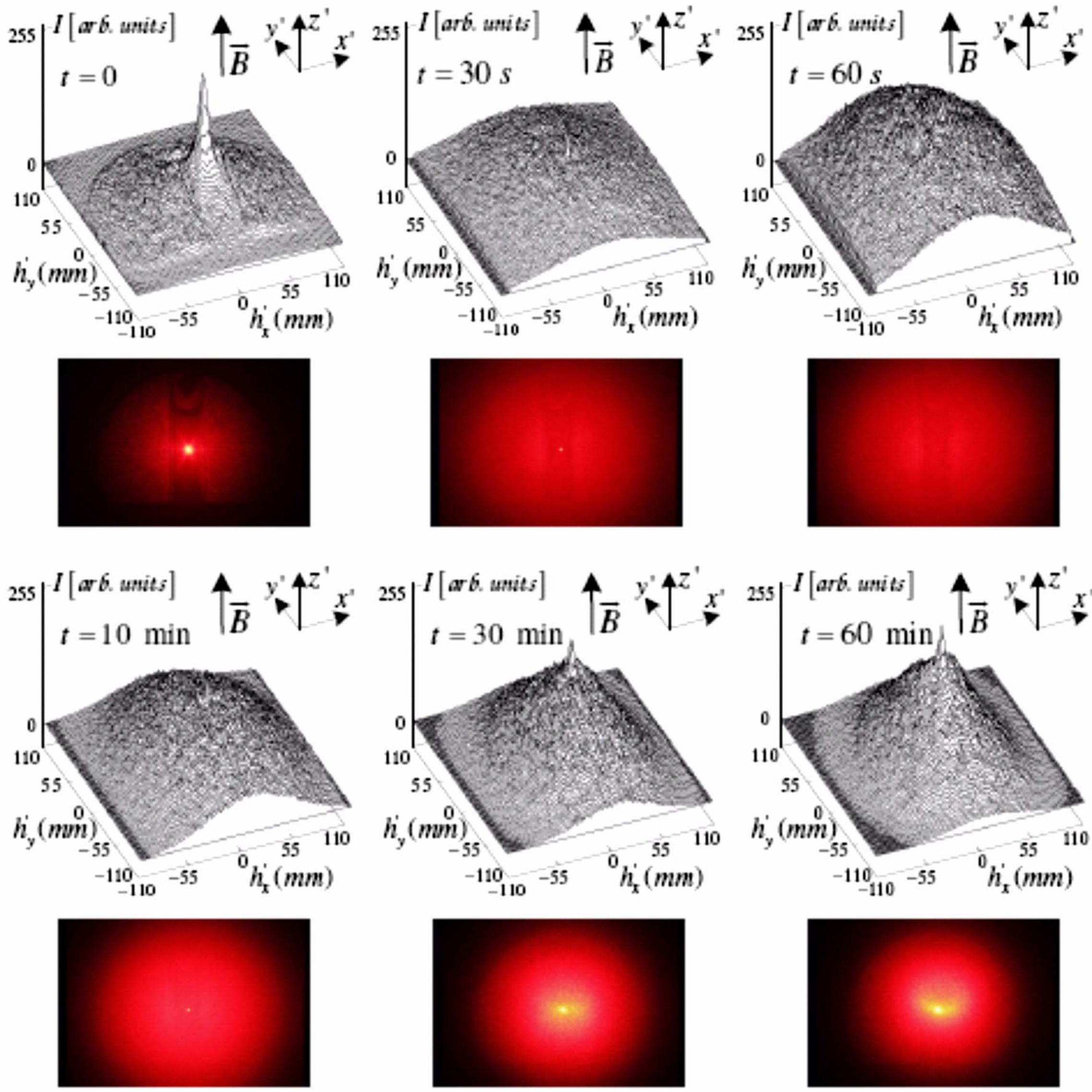

FIG. 3. (Color online) Light scattering patterns from a Fe_3O_4 ferrofluid sample and the corresponding surface plots of the scattered intensity at representative instants of time for incident light propagating parallel to the applied field (i.e., on the $\vec{k}_i \| \vec{B}$ screen). The sample had no prior history in the magnetic field. The magnetic field was turned on at $t=0$, and kept at a steady dc value of 400 G throughout the entire experiment

$$A(h) = 2\frac{I_\perp(h) - I_\|(h)}{I_\perp(h) + I_\|(h)}. \tag{4}$$

A(h) is a measure of the field-induced optical anisotropy which, in the steady state, depends on B.

The results of our experiment are very compatible with this explanation. The angular dependence of the scattered intensity on the $\vec{k}_i \perp \vec{B}$ screen, presented in Fig. 4(a) at $t=30$ s (representative of all the anisotropic scattering patterns in this study) for various magnitudes of the scattering vector $\vec{h}$ reveals a periodic function whose value oscillates between $I_\|(h)$ and $I_\perp(h)$, as predicted by Eq. (2) above. However, the data in our experiments can be fitted by a function of the form given by Eq. (2) only for very small scattering vectors h. At larger scattering vectors, a modified version of this function is needed:

$$I(h,\alpha) = I_0(h)\{1 + A(h)(\sin^{2n}\alpha - 0.5)\}, \tag{5}$$

where $n=n(h)$ is a correction factor that depends on the magnitude of the scattering vector, and has values between 2 and 10 for the data in Fig. 4(a). This can be understood qualitatively by considering that these experiments are in the strong multiple scattering regime. With this correction, we find that the anisotropy factor $A(h)$ introduced above is a good quantitative measure of the scattering anisotropy in our experiments. For a given strength of the steady dc magnetic field $\vec{B}$, $A(h)$ is a function of time, $A=A(h,t)=A_h(t)$. Figure 4(b) shows the angular dependence of the scattered intensity on the $\vec{k}_i \perp \vec{B}$ screen for a scattering vector $h=60$ mm (close to

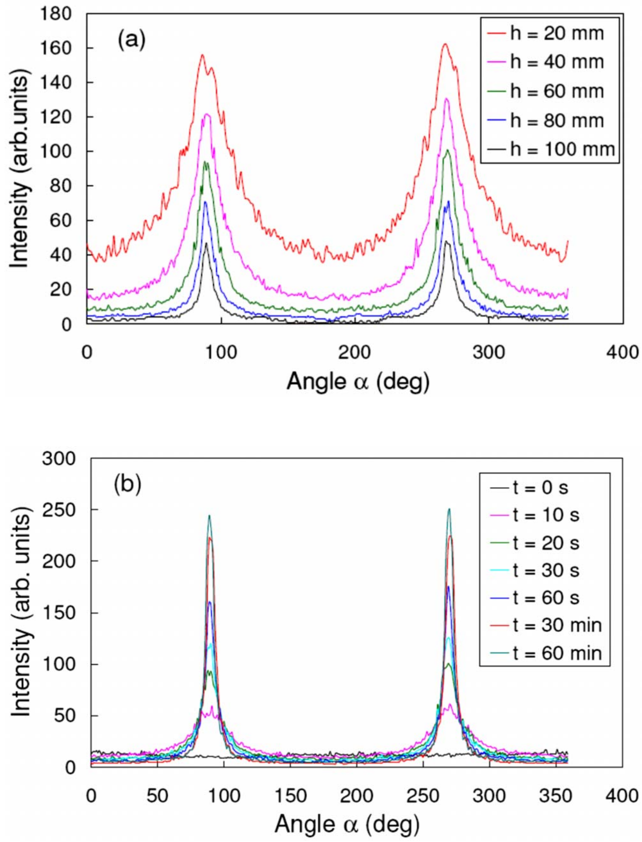

FIG. 4. (Color online) (a) The angular dependence of the scattered intensity on the $\vec{k}_i \perp \vec{B}$ screen, at $t=30$ s for various values of the scattering vector h; from top curve to bottom curve: $h=20$ mm, $h=40$ mm, $h=60$ mm, $h=80$ mm, $h=100$ mm. (b) The angular dependence of the scattered intensity on the $\vec{k}_i \perp \vec{B}$ screen for a scattering vector $h=60$ mm at several instants of time; from top curve to bottom curve: $t=60$ min, $t=30$ min, $t=60$ s, $t=30$ s, $t=20$ s, $t=10$ s, $t=0$ s.

the median value of the scattering vector range in our experiments), at several instants of time. From Figs. 2 and 4(b) it is apparent that the rate of change of the scattering pattern and the rate of change of the optical anisotropy make a transition from a high rate in approximately the first 30 s to a much lower rate after approximately 5 min, and the system approaches a saturated state after approximately 60 min. Since the optical anisotropy is a direct consequence of the aggregation of the Fe_3O_4 nanoparticles in field-induced anisotropic chainlike structures, the kinematics of this optical anisotropy is a direct measure of the kinematics of such chain formation [35]. Figure 5 presents the time dependence of the scattering anisotropy parameter A for several magnitudes of the scattering vector $\vec{h}$. The curves in Fig. 5 generally resemble the field-induced optical transmittance results obtained by Li *et al.* [3] and Martin *et al.* [9]. However, the time dependence in Fig. 5 shows a much faster rise at short times and approaches saturation much faster than the $I(t) = I_\infty / \exp(\tau/t)^\beta$ ($\beta \approx 0.5$) dependence predicted by Martin *et al.* [9] from computer simulation and used to fit their experimental data.

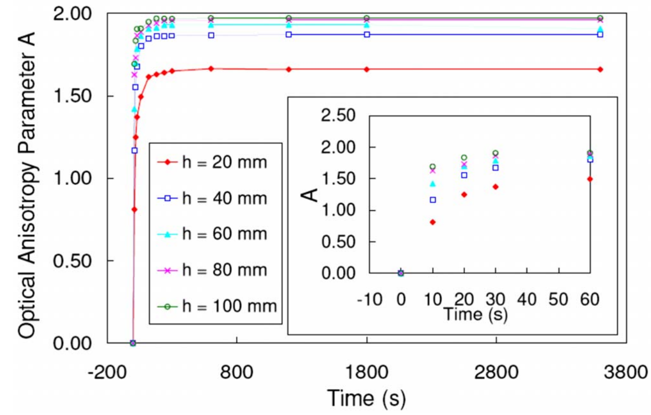

FIG. 5. (Color online) The time dependence of the scattering anisotropy parameter A defined in Eq. (4), corresponding to several values of the scattering vector h. From top curve to bottom curve: $h=100$ mm, $h=80$ mm, $h=60$ mm, $h=40$ mm, and $h=20$ mm. One can identify a very fast evolution shortly after the application of the magnetic field (see the inset), and a significantly slower process at longer times.

We now turn our attention to the scattering patterns on the $\vec{k}_i \| \vec{B}$ screen (Fig. 3) recorded synchronously with the patterns on the $\vec{k}_i \perp \vec{B}$ screen. By obtaining these patterns by introducing the second beam, we add an extra dimension to our investigation, compared to previous studies [3,4,9,24], most of which have confined their observations to the steady-state and/or time-dependent measurements for only one incident beam, propagating either parallel or perpendicular to the applied field. The scattering patterns in Fig. 3, isotropic with respect to the direction of the scattering vector $\vec{h}'$ and having circular symmetry, are in good agreement with the predictions and measurements made in previous static (time-independent) studies [6,24]. In particular, we see evidence of the developing cylindrical symmetry by the characteristic function $\gamma(\vec{r})$ upon the application of a uniform dc magnetic field, as asserted by Kruse *et al.* [4]. Moreover, our synchronous measurements allow the corroboration of the time-corresponding patterns in Figs. 2 and 3 and thus yield additional information by looking at two orthogonal projections, rather than only one, of the same dynamic process of agglomeration of particles in field-induced structures. Indeed, just as for the $\vec{k}_i \perp \vec{B}$ patterns, a relatively fast evolution is observed for approximately the first 30 s after applying the magnetic field, after which the process slows down considerably. However, aside from the cylindrical symmetry induced by the field in the system, and reflected in the isotropic vs anisotropic nature of the two sets of patterns, one notes that the patterns in Fig. 2 evolve monotonically toward a narrow vertical line of light. In contrast, the isotropic patterns in Fig. 3 achieve an almost uniform intensity distribution, with the forward scattered light strongly suppressed to virtually zero forward scattering, only to reverse this trend after approximately 1 min, while still maintaining (to a very good approximation) the radial symmetry of the pattern.

We have repeated these studies with a range of fields from 100 to 300 G to explore how the magnitude of the magnetic

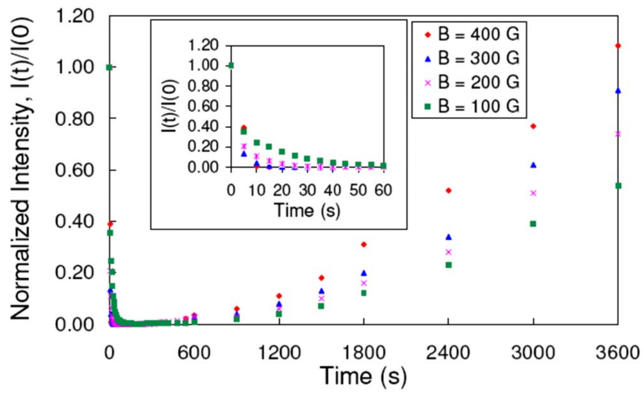

FIG. 6. (Color online) The normalized intensity of the forward scattered light ($h=0$) for the $\vec{k}_i \| \vec{B}$ direction as a function of time at several values of the applied magnetic field.

field affects the nanoparticle dynamics. We find that the patterns at smaller fields are qualitatively similar to those at 400 G, but with slower dynamics. In all cases, we find two distinct regimes, one with a characteristic time of a few minutes after turning on the field, and the second with a much longer time constant of up to a few hours. Our experiments at different fields yield a strong correlation between the fast segment of the time evolution of the scattering patterns and the characteristic time τ_0 needed to achieve zero-forward scattering in the $\vec{k}_i \| \vec{B}$ direction. This decrease and suppression of the forward scattered intensity followed by the reversal of the trend can be clearly observed in Fig. 6, which plots the normalized intensity of the forward scattered light ($h=0$) for the $\vec{k}_i \| \vec{B}$ direction for several values of the applied magnetic field. We plot the magnetic field dependence of the characteristic time τ_0 in Fig. 7, which shows that the time constant varies approximately inversely with H. This functional dependence of τ_0 on H serves as a constraint on possible models for the magnetohydrodynamics of pattern formation for magnetic nanoparticles.

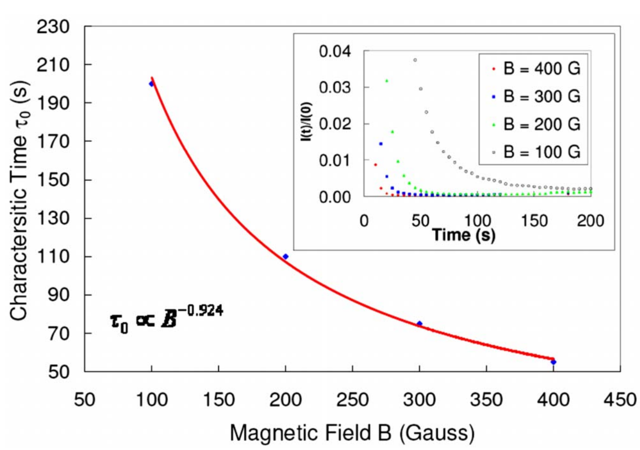

FIG. 7. (Color online) The dependence of the characteristic time τ_0 to zero forward scattered intensity in the $\vec{k}_i \| \vec{B}$ direction on the magnitude of the applied magnetic field. The best fit line reveals an approximate inverse dependence of τ_0 with B. The inset shows a blow up of the normalized forward scattered intensity at short times.

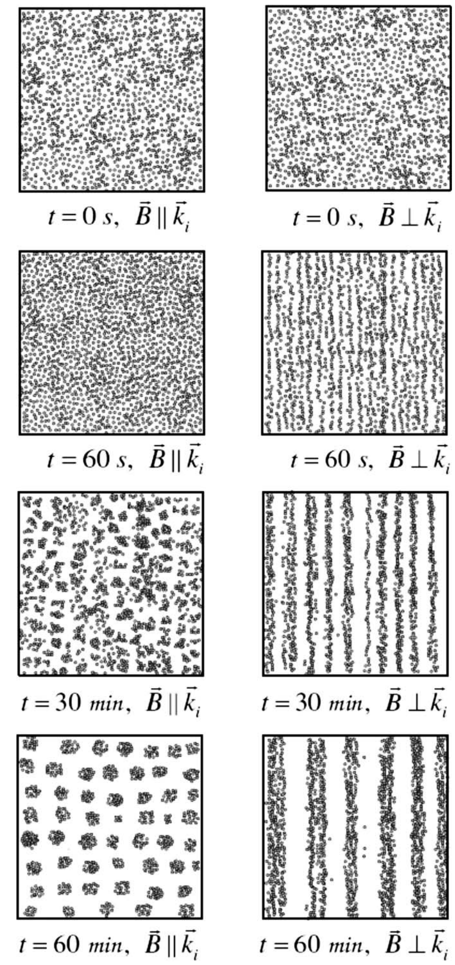

FIG. 8. Schematic of the proposed nanoparticles aggregation patterns as viewed by a light beam propagating along the field lines ($\vec{k}_i \| \vec{B}$) and perpendicular to the field lines ($\vec{k}_i \perp \vec{B}$). A rough time correspondence with the patterns in Figs. 2 and 3 is included.

B. Chain formation and coarsening

Our experimental observations outlined in Sec. III A are in good general agreement with the expanded Halsey-Toor model of chain formation and coarsening through lateral coalescence of chains [7–9]. The patterns in Figs. 2 and 3 and the time dependence of the forward scattered intensity in Fig. 6 can be explained through an aggregation process that takes the ferrofluid through a sequence of particle agglomerations as presented schematically in Fig. 8. In the absence of the magnetic field (occurring at $t<0$ in this experiment), the particles are randomly distributed in the ferrofluid. At very short times after turning the magnetic field on (on the order of several seconds), individual nanoparticles will join irreversibly through magnetic interaction, forming rather short chains aligned along the field lines. Once these initial short chain-aggregates are formed, tip-to-tip aggregation takes place, i.e., aggregation of shorter parallel chains (placed approximately along the same line) into longer chains [11]. Considering the small characteristic dimension of these initial aggregates (with an average cross section of only one particle), and the fact that a tip-to-tip aggregation involves mostly longitudinal movement (diffusion) of the chains, one can expect this process to be reasonably fast, as reflected by the evolution of the scattering patterns at short times (during the first 30 s in Figs. 2 and 3 for a 400 G field) in our experiments. While this leads to an ordering of the ferrofluid viewed perpendicular to the field lines, a laser beam propagating parallel to the field lines will see an increased disorder in the system. This can be explained in view of the long light path through the sample, and considering nonrigid chains affected by thermal fluctuations and defects. This increased disorder results in a stronger but isotropic scattering, which explains the patterns in Fig. 3 at $t=30$ s and $t=60$ s, and the initial decrease in the forward scattered intensity on the $\vec{k}_i \| \vec{B}$ screen presented in Fig. 6. On the other hand, at longer times ($t>5$ min in our experiments), the chains coarsen through lateral aggregation to form thicker columns or more complex formations that maintain a longitudinal alignment with the magnetic field. Such lateral aggregation can happen through lateral interaction between nearby chains that are shifted with respect to each other such that the individual magnetic moments in the two chains are interleaved [8]. In addition, thermal fluctuations and topological defects in chains due to nanoparticle shape and size polydispersity will also contribute to lateral aggregation [8]. In view of the weaker lateral interaction and slower diffusion in a direction perpendicular to the longitudinal direction of the chains, one can expect this motion to be significantly slower, as revealed by the slower evolution of the scattering patterns in Figs. 2 and 3 at longer times ($t>5$ min). The lateral aggregation and coalescence of chains into thicker columns results in a smaller cross section for the scattering of light propagating parallel to the magnetic field, and thus more light will be transmitted through the sample. This behavior has been predicted through computer simulations by Martin *et al.* [9] and confirmed through the experimental measurements of light attenuation by Li *et al.* [3] and Martin *et al.* [9]. We note that a similar two-stage (fast-process–slow-process) evolution was observed by Hoffmann and Köhler [36] and Kellner and Köhler [37] for light-induced cluster formation in ferrofluids. In order to test whether light-induced clustering could be relevant in our system, we repeated our experiment using a red He-Ne laser (632.8 nm, 10 mW, 1 mm beam diameter) and a green He-Ne laser (543 nm, 1 mW, 1 mm beam diameter). We did not detect any light-induced changes in the intensity or pattern of the transmitted light in the absence of a magnetic field for observation times as long as 18 h, for either of the two wavelengths. This provides strong direct evidence for both the lack of light-induced structures in our ferrofluid and also confirms the stability of the colloidal suspension in the absence of the magnetic field.

Rather different optical anisotropy results are exhibited by the ferrofluid sample in our experiments after the field is switched off, as compared to the field on transition. Our preliminary measurements show that the system does not become isotropic almost instantaneously, as observed in other studies [9]. Although the dissociation and segregation process appears to be much faster than the aggregation process, particularly at short times ($t<30$ s), it takes about five minutes for the ferrofluid to completely regain the isotropic state. During these five minutes the ferrofluid evolves through states producing not only anisotropic light scattering patterns in both $\vec{k}_i \perp \vec{B}$ and $\vec{k}_i \| \vec{B}$ directions, but also exhibiting an interesting phenomenon of angular fluctuation of the patterns. We are in the process of understanding and analyzing the kinematics in terms of the decoarsening of the thick columns of chains, defragmentation of longer chains into the smaller segments, and finally into individual nanoparticles.

IV. CONCLUSIONS

In this paper we have presented the results of simultaneous light scattering measurements for two orthogonal He-Ne laser beams propagating through a ferrofluid consisting of 6-nm-sized Fe_3O_4 nanoparticles, under the influence of an external dc magnetic field. From the periodic nature of the scattered intensity, we determined the time-dependent optical anisotropy parameter which increases rapidly at short times and much slower at longer times, toward a saturation state. The intensity of the forward scattered light parallel to the applied field was found to have nonmonotonic time dependence, dropping off sharply to virtually zero forward scattering at short times then increasing to values that are strongly field dependent at long times. The characteristic time to zero forward scattering—a measure of the time length of the fast process—was found to vary inversely with the magnitude of the applied magnetic field. The existing models by Halsey and Toor, Martin *et al.*, and Furst and Gast relating to the chain formation and subsequent chain coarsening were used to explain our results. Preliminary results for the field on to field off transition have revealed a dissociation process of the chainlike structures approximately ten times faster than the aggregation process. The interesting feature of angular fluctuations of the anisotropic scattering patterns after switching off the field suggests the presence of some angular field during the dissociation of the chains and will be the subject of future investigation.

ACKNOWLEDGMENTS

The authors at Wayne State University acknowledge the support of their work by the donors of the American Chemical Society (PRF Grant No. 46160-G10), Richard J. Barber Funds for Interdisciplinary Research and the Institute for Manufacturing Research at Wayne State University.

[1] D. Heinrich, A. R. Goni, and C. Thomsen, J. Chem. Phys. **126**, 124701 (2007).
[2] R. Tackett, C. Sudakar, R. Naik, G. Lawes, C. Rablau, and P. P. Vaishnava, J. Magn. Magn. Mater. **320**, 2755 (2008).
[3] J. Li, X. D. Liu, Y. Q. Lin, Y. Huang, and L. Bai, Appl. Phys. B **82**, 81 (2006).
[4] T. Kruse, H. G. Krauthauser, A. Spanoudaki, and R. Pelster, Phys. Rev. B **67**, 094206 (2003).
[5] S. Melle, O. G. Calderon, M. A. Rubio, and G. G. Fuller, Phys. Rev. E **68**, 041503 (2003).
[6] S. Melle, Ph.D. thesis Spanish National Open University (UNED), Madrid, Spain, 2002, and references therein.
[7] T. C. Halsey and W. Toor, Phys. Rev. Lett. **65**, 2820 (1990).
[8] E. M. Furst and A. P. Gast, Phys. Rev. E **62**, 6916 (2000).
[9] J. E. Martin, K. M. Hill, and C. P. Tigges, Phys. Rev. E **59**, 5676 (1999).
[10] J. E. Martin, J. Odinek, T. C. Halsey, and R. Kamien, Phys. Rev. E **57**, 756 (1998).
[11] S. Fraden, A. J. Hurd, and R. B. Meyer, Phys. Rev. Lett. **63**, 2373 (1989).
[12] D. Smith, and K. L. Stokes, Opt. Express **14**, 5746 (2006).
[13] J. P. Huang, Z. W. Wang, and C. Holm, Phys. Rev. E **71**, 061203 (2005).
[14] A. O. Ivanov, Z. Wang, and C. Holm, Phys. Rev. E **69**, 031206 (2004).
[15] V. S. Mendelev and A. O. Ivanov, Phys. Rev. E **70**, 051502 (2004).
[16] T. Kruse, A. Spanoudaki, and R. Pelster, Phys. Rev. B **68**, 054208 (2003).
[17] Z. Wang, C. Holm, and H. W. Muller, Phys. Rev. E **66**, 021405 (2002).
[18] M. Carmen Miguel and R. Pastor-Satorras, Phys. Rev. E **59**, 826 (1999).
[19] R. Tao and Q. Jiang, Phys. Rev. Lett. **73**, 205 (1994).
[20] W. R. Toor and T. C. Halsey, Phys. Rev. A **45**, 8617 (1992).
[21] P. C. Morais, K. Skeff Neto, A. F. Bakuzis, M. F. Da Silva, and N. Buske, IEEE Trans. Magn. **38**, 3228 (2002).
[22] F. Donatini, D. Jamon, J. Monin, and S. Neveu, IEEE Trans. Magn. **35**, 4311 (1999).
[23] B. Payet, F. Donatini, and G. Noyel, J. Magn. Magn. Mater. **201**, 207 (1999).
[24] Y. H. Hwang and X.-l. Wu, Phys. Rev. E **49**, 3102 (1994).
[25] M. F. da Silva and A. M. Figueiredo Neto, Phys. Rev. E **48**, 4483 (1993).
[26] J. M. Ginder, Phys. Rev. E **47**, 3418 (1993).
[27] G. N. Rao, Y. D. Yao, Y. L. Chen, K. T. Wu, and J. W. Chen, Phys. Rev. E **72**, 031408 (2005).
[28] G. L. J. A. Rikken and B. A. van Tiggelen, Nature (London) **381**, 54 (1996).
[29] A. Sparenberg, G. L. J. A. Rikken, and B. A. van Tiggelen, Phys. Rev. Lett. **79**, 757 (1997).
[30] F. A. Pinheiro, A. S. Martinez, and L. C. Sampaio, Phys. Rev. Lett. **84**, 1435 (2000).
[31] R. V. Mehta, R. Patel, and R. V. Upadhyay, Phys. Rev. B **74**, 195127 (2006).
[32] A. K. Vuppu, A. A. Garcia, and M. A. Hayes, Langmuir **19**, 8646 (2003).
[33] P. P. Vaishnava, R. Tackett, A. Dixit, C. Sudakar, R. Naik, and G. Lawes, J. Appl. Phys. **102**, 063914 (2007).
[34] H. C. van de Hulst, *Light Scattering by Small Particles* (Dover Publications, New York, 1981).
[35] V. Socoliuc *et al.*, J. Magn. Magn. Mater. **191**, 241 (1999).
[36] B. Hoffmann and W. Köhler, J. Magn. Magn. Mater. **262**, 289 (2003).
[37] R. R. Kellner and W. Köhler, J. Appl. Phys. **97**, 034910 (2005).